Nanoscale

RSC Publishing

PAPER

View Article Online
View Journal | View Issue

# Graphene oxide embedded sandwich nanostructures for enhanced Raman readout and their applications in pesticide monitoring†

Cite this: *Nanoscale*, 2013, **5**, 3773

Lulu Zhang,[ab] Changlong Jiang*[b] and Zhongping Zhang*[ab]

Analytical techniques based on surface-enhanced Raman scattering (SERS) suffer from a lack of reproducibility and reliability, thus hampering their practical applications. Herein, we have developed a SERS-active substrate based on a graphene oxide embedded sandwich nanostructure for ultrasensitive Raman signal readout. By using this novel Au@Ag NPs/GO/Au@Ag NPs sandwich nanostructure as a SERS substrate, the Raman signals of analytes were dramatically enhanced due to having plenty of hot spots on their surfaces and the unique structure of the graphene oxide sheets. These features make the sandwich nanostructured film an ideal SERS substrate to improve the sensitivity, reproducibility and reliability of the Raman readout. The sandwich nanostructure film can be applied to detect rhodamine-6G (R6G) with an enhancement factor (EF) of $\sim 7.0 \times 10^7$ and the pesticide thiram in commercial grape juice with a detection limit of as low as 0.1 μM (0.03 ppm), which is much lower than the maximal residue limit (MRL) of 7 ppm in fruit prescribed by the U.S. Environmental Protection Agency (EPA). The GO embedded sandwich nanostructure also has the ability to selectively detect dithiocarbamate compounds over other types of agricultural chemical. Furthermore, spiked tests show that the sandwich nanostructure can be used to monitor thiram in natural lake water and commercial grape juice without further treatment. In addition, the GO enhanced Raman spectroscopic technique offers potential practical applications for the on-site monitoring and assessment of pesticide residues in agricultural products and environments.

Received 4th February 2013
Accepted 9th March 2013

DOI: 10.1039/c3nr00631j

**www.rsc.org/nanoscale**

## 1 Introduction

Since its first observation on a rough Ag electrode thirty years ago, the surface-enhanced Raman scattering (SERS) spectroscopic technique has become one of the most widely used spectroscopic tools for the identification and detection of chemical and biological species owing to its integration of high sensitivity, unique spectroscopic fingerprint, and non-destructive data acquisition.[1] Up to now, most of the SERS platforms are noble metal colloidal nanoparticles (NPs) where enormous Raman enhancement factors could be obtained in areas of "hot spots" from the locations of colloidal aggregations.[2] However, hot spots in these systems are randomly distributed and it is very difficult for the targets to enter the conjunctions among the aggregated NPs. Therefore, it is highly desirable to fabricate ultrasensitive, reproducible, and uniform SERS-active substrates for ultrasensitive Raman detection. In recent years, various approaches have been developed to fabricate highly SERS-active substrates to yield uniform and reproducible Raman signals and almost all of the SERS substrates are made from pure metallic nanostructures.[3]

Graphene is a perfect 2D material with a monolayer of carbon atoms packed into a honeycomb crystal plane, which is uniform and has previously been reported to play a role as a Raman enhancement substrate.[4] On the other hand, graphene oxide (GO), the oxidized state of graphene, also attracts much interest in SERS applications because of its specific surface structures.[5] Molecules can easily form a unified orientation on it collectively due to the flatness of the graphene oxide surface. This allows measurement of the Raman signal from molecules with a unified orientation, rather than an average effect from many randomly oriented molecules. Graphene oxide enlarges the molecular orientation change and makes this effect easier to observe.[6] Grapheme oxide has a high adsorption capacity toward aromatic compounds and pesticides,[7] and some methods have been developed to synthesize nanohybrid structures of GO with noble metal NPs for SERS applications.[5] To obtain a unified GO–metal nanohybrid structure, it is better to fix it on a solid substrate for stable, reliable and uniform Raman signal readout, and most substrate-based structures consist of graphene (or GO) and Au (or Ag) NPs.[8] It is reported that

[a]*Department of Chemistry, University of Science & Technology of China, Hefei, Anhui, 230026, China*

[b]*Institute of Intelligent Machines, Chinese Academy of Sciences, Hefei, Anhui, 230031, China. E-mail: cljiang@iim.ac.cn; zpzhang@iim.ac.cn*

† Electronic supplementary information (ESI) available. See DOI: 10.1039/c3nr00631j

silver-coated gold nanoparticles (Au@Ag NPs) in solution have individual particle-based SERS ability toward some kinds of pesticides, and the Au@Ag NPs can also be synthesized to have uniform size and shape using Au NPs as seeds, which are difficult to obtain for Ag NPs.[9]

Herein, we report a novel sandwich nanostructure composed of GO nanosheets and Au@Ag NPs for enhanced Raman signal readout. The GO embedded sandwich structure was used as the SERS-active substrate to detect rhodamine 6G (R6G) with an enhancement factor of as high as $\sim 7.0 \times 10^7$. Moreover, the as-fabricated SERS substrate can be employed to enhance the Raman signals of thiram, showing a detection limit as low as 0.03 ppm, which is much lower than the maximal residue limit (MRL) of 7 ppm in fruit prescribed by the U.S. Environmental Protection Agency (EPA).

Dithiocarbamates are a group of organosulfur compounds extensively used for a wide range of applications in agriculture and industry.[10] Among them, thiram (bis-(dimethyldithiocarbamoyl)disulfide), a dithiocarbamate fungicide, is one of the most largely used worldwide in agriculture as a fungicide and animal repellent. Moreover, the toxicity induced by exposure to thiram can lead to serious skin and eye illnesses, as well as damage to the liver due to the carbon disulfide release from thiram.[11] Conventional analyses of thiram are usually performed with colorimetry, chromatography, spectrophotometry, polarography and other electrochemical methods.[12] However, these techniques require sophisticated sampling, prior separation/extraction and preconcentration procedures, and thus they are complicated, high-cost and time-consuming. It's very urgent to develop simple, rapid, ultrasensitive analytical techniques for the on-site analysis of trace pesticide residues to improve environmental and agricultural safety. The SERS technique based on the self-assembled sandwich nanostructure shows potential as a complementary method for the sensitive and rapid detection of dithiocarbamate chemicals.

## 2 Experimental section

### 2.1 Materials

Thiram, chlorpyrifos, imidacloprid, ethoprophos, 2,4-dichlorophenoxyacetic acid, parathion-ethyl, atrazine, rhodamine-6G (R6G), 3-aminopropyltriethoxysilane (APTES) and poly(ethyleneimine) (PEI, $M_w \approx 25\,000$) were purchased from Sigma. Graphite flakes (325 mesh) were provided by Alfa Aesar. Silver nitrate ($AgNO_3$), sodium citrate ($Na_3C_6H_5O_7 \cdot 2H_2O$, 99.8%), chloroauric acid ($HAuCl_4 \cdot 4H_2O$, 99.9%) and sodium diethyldithiocarbamate (AR) were obtained from the Sinopharm Chemical Reagent Co., Ltd. All reagents were used without further purification. Ultrapure water (18 MΩ) was produced using a Millipore water purification system and used for all solution preparations.

### 2.2 Synthesis of citrate-stabilized Au, Au@Ag, and Ag nanoparticles

Typically, 0.25 mL of 0.1 M $HAuCl_4$ was added to 100 mL of ultrapure water and then heated to boiling under magnetic stirring. After quickly injecting 1.5 mL of 1% trisodium citrate, the mixed solution was refluxed for ~30 min until it became wine red and the Au NPs were synthesized. 4 mL of 1% trisodium citrate was rapidly injected into the above boiling solution. Then 17 mL of 1 mM $AgNO_3$ was added dropwise into the above mixture at a rate of one drop per 30 s. Silver nitrate was reduced by trisodium citrate and the resultant silver continuously grew on the surface of the Au seeds. After the wine red of solution changed to orange yellow, the solution was stirred for 30 min and the Au@Ag NPs were obtained. Meanwhile, Ag NPs were prepared by the reduction of $AgNO_3$ with trisodium citrate in water.[13]

### 2.3 Fabrication of the GO embedded sandwich nanostructure

The GO nanosheets were first prepared from natural graphite flakes by a modified Hummers method.[14] Au@Ag NPs were assembled on a silicon substrate in the following procedure: first, a silicon substrate was cleaned by sequential ultrasonication in acetone, ethanol, and deionized water for 15 min in sequence and then treated with $H_2SO_4$–$H_2O_2$ (3 : 1 (v/v) $H_2SO_4$ (98%)–$H_2O_2$ (30%)) at 90 °C for 30 min to derive a hydroxyl surface. After thoroughly rinsing with Milli-Q ultrapure water and ethanol, the cleaned silicon substrate was dried in air. Second, the silicon substrate was immersed in a 10% solution of APTES in ethanol for 18 h to silanize the substrate, which was then extensively rinsed with ethanol to remove unbound monomers from the surface and dried in air. Third, the silane modified silicon substrate was submerged in colloidal Au@Ag NPs for 12 h, resulting in the formation of a layer of Au@Ag NPs on the silicon surface. The silicon substrate with a layer of Au@Ag NPs was coated with PEI by immersing it in 4 mg $mL^{-1}$ positively charged PEI solution for 2 h. After being washed with pure water, the PEI-coated substrate was dipped into a 0.125 mg $mL^{-1}$ GO solution for 2 h to modify the substrate with GO. The substrate was covered with PEI again over the GO layer. Finally, after being washed with pure water, the substrate was again submerged in colloidal Au@Ag NPs, resulting in the formation of the Au@Ag NPs/GO/Au@Ag NPs sandwich structure.

### 2.4 Raman detection of R6G in ethanol

10 μL aliquots of different concentrations of R6G in ethanol were dispersed on the as-prepared substrates and dried in an air for SERS detection. The Raman spectra were recorded using a 532 nm laser with 1 mW power and a 50× objective (1 $\mu m^2$ spot). The integral time was 0.5 s and the slit aperture was 50 μm.

### 2.5 Raman detections of pesticides in ethanol and thiram in spiked samples

For the detection of thiram in ethanol, 10 μL aliquots of different concentrations of thiram in ethanol were dispersed on the as-prepared substrates; other pesticides were also detected using the same method. For the detection of thiram in spiked samples, 100 μL of the spiked sample solution was diluted in ethanol to 1 mL, then 10 μL of the diluted solution was dropped

 

onto the substrate. The Raman spectra were recorded using 532 nm laser with 8 mW power and a 50× objective (1 $\mu m^2$ spot). The integral time was 2 s and the slit aperture was 50 μm.

### 2.6 Instruments

Absorption spectra of the colloidal Au NPs, Ag NPs, Au@Ag NPs and GO solution were measured using a Shimadzu UV-2550 spectrometer. Optical photographs were taken by a Canon-350D digital camera. The structures of the samples were characterized using field-emission scanning microscopy (FE-SEM, Sirion 200) and transmission electron microscopy (TEM, JEOL 2010). Atomic force microscopy (AFM) images were recorded on a DI Innova. Zeta-potential measurements were conducted with a Zetasizer 3000 HSA. Raman measurements were conducted with a ThermoFisher DXR Raman microscope equipped with a CCD detector with an excitation wavelength of 532 nm. The laser beam was focused to a spot of about 1 $\mu m^2$ by a 50× microscope objective.

## 3 Results and discussion

### 3.1 Fabrication and characterization of the Au@Ag NPs/GO/Au@Ag NPs sandwich structure

The fabrication procedure of the graphene oxide embedded sandwich structure is schematically illustrated in Fig. 1. The GO nanosheets were first prepared from natural graphite flakes by a modified Hummers method. The silicon substrate was modified by silanization with APTES, resulting in an amino-terminated silane monolayer on its surface for further chemical conjugation with the Au@Ag NPs. Next, the APTES-modified substrate was immersed in a colloidal suspension of Au@Ag NPs, leading to a layer of Au@Ag NP film on the substrate (step 1). Then, the substrate was submerged in a positively charged PEI solution to endow positive charge on the surface. The PEI-coated substrate was then immersed in a GO solution to modify the substrate with GO (step 2). The silicon substrate was again covered with another layer of PEI on the GO. Finally, the substrate was submerged in colloidal Au@Ag NPs, resulting in a graphene oxide embedded sandwich structure (step 3). The as-obtained GO-embedded sandwich structure can serve as a SERS-active substrate for Raman detection with high sensitivity, good reproducibility and high reliability due to having plenty of hot spots on its surface and the unique structure of the graphene oxide sheets.

Uniform Au@Ag NPs were synthesized in aqueous solution *via* seed growth through consecutive two-step reactions. First, Au NP colloids with a size of 30 nm were prepared by the chemical reduction of chloroauric acid with sodium citrate. Subsequently, $AgNO_3$ solution was mixed into the Au NP colloids under vigorous stirring. Due to the match in the crystalline lattices of Ag and Au, the resultant Ag metal was selectively grown on the Au cores and the core–shell Au@Ag NPs were obtained (Fig. S1, ESI†), accompanied by an obvious color change from wine red to orange. Fig. 2 shows the SEM images of the samples obtained in above mentioned steps. Au@Ag NPs were first assembled on the silicon substrate (Fig. 2a). The Au@Ag NP film was coated with a positively charged poly(ethyleneimine) (PEI) layer and then grafted with the negatively charged GO (Fig. 2b). It was difficult to identify the GO under SEM due to its extremely small thickness. The crumpled sheet morphology of GO observed in the enlarged SEM image indicates that GO was successfully grafted onto the surface (Fig. S2, ESI†). The as-obtained film was further deposited with another layer of Au@Ag NPs, showing a higher density compared with the first layer of Au@Ag NPs assembled on the silicon substrate, resulting in a graphene oxide embedded sandwich structure (Fig. 2c).

Raman measurements were also conducted to characterize the as-obtained samples. As shown in Fig. 2d, only the strong Raman scattering signal of silicon is observed on the Au@Ag NP film, while obvious Raman peaks of the D band and G band of GO are observed on the GO coated Au@Ag NP film and Au@Ag NPs/GO/Au@Ag NPs sandwich structure. Raman peaks of GO recorded from 10 random spots on the GO coated Au@Ag NP film are almost identical, which demonstrates the good uniformity of GO grafted on the PEI-coated Au@Ag NP film

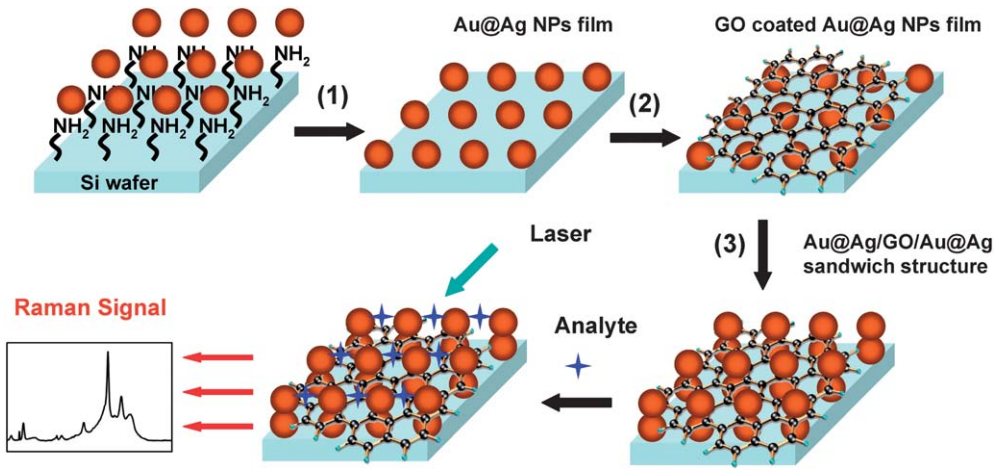


**Fig. 1** A schematic illustration of the fabrication process of the graphene oxide embedded sandwich structure and its application in SERS.

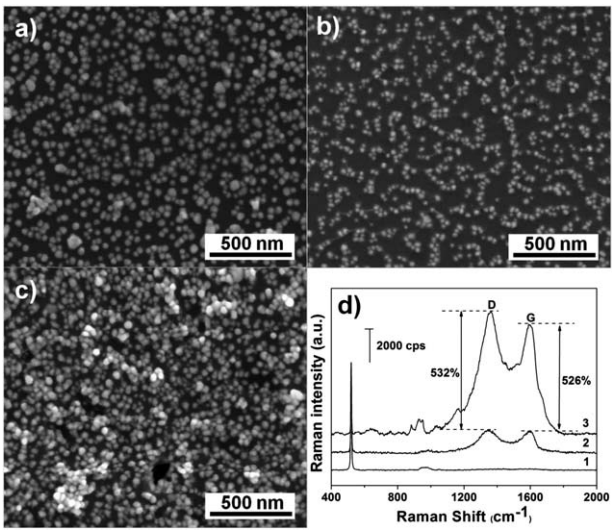


**Fig. 2** SEM images of (a) assembled Au@Ag NP film, (b) GO coated Au@Ag NP film and (c) Au@Ag NPs/GO/Au@Ag NPs sandwich structure. (d) Raman signals of the Au@Ag NP film (curve 1), GO coated Au@Ag NP film (curve 2) and Au@Ag NPs/GO/Au@Ag NPs sandwich structure (curve 3).

(Fig. S3a, ESI†). The samples were further checked with AFM (Fig. S4, ESI†). AFM images reveal the uniform surface morphology after coating GO on the Au@Ag NP film. After the second layer of the Au@Ag NPs was loaded, the D band and G band of GO can still be clearly identified from the Raman spectrum of Au@Ag NPs/GO/Au@Ag NPs, which confirms the successful fabrication of the Au@Ag NPs/GO/Au@Ag NPs sandwich structure. The D band and G band intensities of GO are both significantly enhanced in Au@Ag NPs/GO/Au@Ag NPs, which could be attributed to the coupled surface plasmon resonance (SPR) absorption of the Au@Ag NPs on GO.[15]

The PEI layer played a crucial role in the modification of the Au@Ag NP film with GO. PEI is positively charged at a pH <10.5 in aqueous solution due to a large number of basic amino groups at the polymer chains.[16] The PEI-modified Au@Ag NP film had a positive charge on its surface, and the negatively charged GO could be tightly absorbed onto it through the electrostatic force (Table S1, ESI†). When non-PEI-coated Au@Ag NP film was used under the same experimental conditions, only unstable Raman signals of GO were obtained, which could be ascribed to the non-uniform adsorption of GO on the surface of Au@Ag NP film (Fig. S3b, ESI†). Through the counter-charge interaction based self-assembly strategy, the Au@Ag NPs/GO/Au@Ag NPs sandwich structure was obtained.

### 3.2 SERS properties of the Au@Ag NPs/GO/Au@Ag NPs sandwich structure

R6G, one of the widely used standard probes for the evaluation of SERS performance, was chosen to probe the SERS effect of the GO embedded sandwich structure. The strong Raman peaks at 612 $cm^{-1}$, 774 $cm^{-1}$, 1360 $cm^{-1}$, 1509 $cm^{-1}$, and 1650 $cm^{-1}$ are in good agreement with previous reports on pure R6G.[17] The Raman signals can still be observed even when its concentration decreased to as low as 1 nM (Fig. S5a, ESI†). Raman spectra of R6G molecules ($1 \times 10^{-7}$ M) were taken from 15 randomly selected places on the substrate (Fig. S5b, ESI†), and the relative standard deviation (RSD) of the 612 $cm^{-1}$ peak intensities of R6G is 8.4%, demonstrating the good uniformity of the substrate. To probe the Raman scattering effect of the sandwich structure, Raman spectra were collected by adding R6G ($1 \times 10^{-7}$ M) onto the surface of the bare silicon substrate (Si), Au@Ag NP film, two layers of Au@Ag NPs on a silicon substrate modified with PEI instead of GO (Au@Ag NPs/PEI/Au@Ag NPs), and the Au@Ag NPs/GO/Au@Ag NPs film, respectively. As shown in Fig. 3, no Raman signal of R6G is detected on the Si substrate, while strong Raman signals of R6G are monitored on the other three substrates. Compared with the Au@Ag NP film, the Raman signals of R6G were enhanced about 3 times on the Au@Ag NPs/PEI/Au@Ag NPs and 5 times on the Au@Ag NPs/GO/Au@Ag NPs film, respectively. Au NPs and Ag NPs instead of Au@Ag NPs were also used to prepare the GO embedded sandwich nanostructure, showing the different Raman enhancements of R6G (Fig. S6, ESI†).

The SERS enhancement factors (EF) for R6G on the Au@Ag NPs/GO/Au@Ag NPs sandwich structure film can be calculated according to the equation $EF = (I_{SERS}/I_{bulk})(N_{bulk}/N_{surface})$, where $I_{SERS}$ and $I_{bulk}$ are the peak intensities of 1 nM R6G on the sandwich structure and 0.1 M R6G on a silicon substrate at 612 $cm^{-1}$, respectively (Fig. S7, ESI†). $N_{SERS}$ and $N_{bulk}$ are the number of R6G molecules excited by the laser beam on the sandwich structure and silicon substrate, respectively. The calculated EF of the sandwich structure is about $7.0 \times 10^7$. The experimental results confirm that the GO embedded sandwich structure has high sensitivity, uniformity, and good reproducibility as the substrate for Raman applications.

### 3.3 SERS detection of thiram

The sandwich structure was further applied for the detection of trace thiram, a widely used sulfur-containing pesticide. Fig. 4a

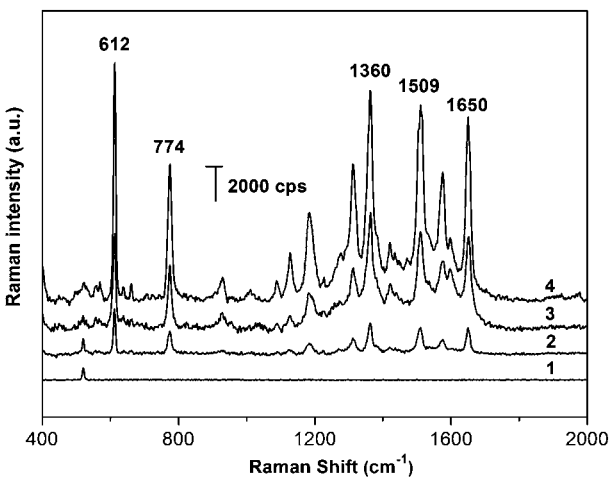


**Fig. 3** SERS spectra of $10^{-7}$ M R6G in ethanol on Si (curve 1), Au@Ag NP film (curve 2), Au@Ag NPs/PEI/Au@Ag NPs (curve 3), and Au@Ag NPs/GO/Au@Ag NPs (curve 4).

 

shows the Raman spectra of thiram in ethanol with concentrations increasing from $1.0 \times 10^{-7}$ to $1.0 \times 10^{-5}$ M using the sandwich structure as the substrate. The intensity of Raman peaks of thiram located at 560 $cm^{-1}$, 1148 $cm^{-1}$, 1386 $cm^{-1}$, 1507 $cm^{-1}$ increase with the thiram concentration, whereas the intensities of the D and G bands of GO nearly remain unchanged. Fig. 4b reflects the relationship between SERS intensity at 560 $cm^{-1}$ and the concentrations of the thiram in ethanol. Even at the 0.1 μM (0.03 ppm) level, signals of thiram can still clearly be noticed. The detection limit of thiram is lower than the maximal residue limit of 7 ppm in fruit prescribed by the U.S. Environmental Protection Agency (EPA).

### 3.4 SERS selectivity of the Au@Ag NPs/GO/Au@Ag NPs sandwich structure for detecting dithiocarbamate

The selectivity of the present detection system for thiram was also examined among a wide variety of agricultural chemicals, including 2,4-dichlorophenoxyacetic acid, imidacloprid, chlorpyrifos, ethoprophos, parathion-ethyl, atrazine and an analog of thiram (sodium diethyldithiocarbamate) (Fig. S8, ESI†). Fig. 5 shows the SERS spectra of these agricultural chemicals obtained by following the same procedure as for thiram. It can be seen that the Raman signals of dithiocarbamates could be easily detected, while the other types of compounds did not show SERS signals at the same concentration. As reported in the literature, the thiram molecule easily forms a resonated radical structure when interacting with a metal surface such as Ag NPs, leading to the S–S bond cleavage of thiram, which gives rise to two dimethyl residues that are strongly adsorbed on the Ag NPs by replacing the original citrate ligands at the surface of the Ag NPs.[18] The strong adsorption takes place *via* the SCS group through a bidentate complex with Ag atoms. The adsorption of the sulfur-containing pesticide on the Au@Ag NPs of the sandwich structure provides the best possibility for their identification and detection by SERS techniques. Furthermore, SERS bands with specific frequencies could be obtained from different dithiocarbamate compounds. This can be used to distinguish between different dithiocarbamates. These results indicate that the present sensing system exhibits a high selectivity for thiram and could be applied for the detection of thiram in environmental samples.

### 3.5 Spike test of thiram in real samples

The high Raman sensitivity of the GO embedded sandwich structure is particularly suitable for the practical monitoring the residual pesticide molecules in various environments. We present the unusual but important applications of the sandwich structure for the identification and detection of pesticide residues, which when using other techniques are either undetectable or need complicated sample pretreatments. The spike tests were applied to different matrices, including grape juice, ultrapure water and real lake water. The real lake water was collected from a local lake and the grape juice was bought from a local market. The thiram solution with different concentrations was spiked into the grape juice, ultrapure water and real lake water. For the SERS experiment, in order

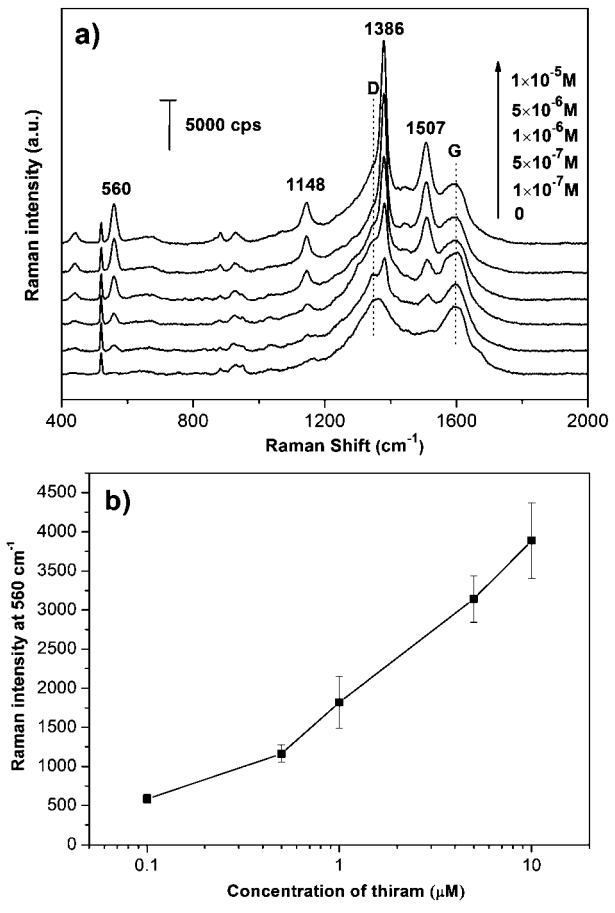


**Fig. 4** (a) SERS spectra of thiram in ethanol of various concentrations on a Au@Ag NPs/GO/Au@Ag NPs sandwich structure. The peaks marked by D and G are the D band (~1350 $cm^{-1}$) and G band (~1595 $cm^{-1}$) of GO. (b) The intensities of SERS signals at 560 $cm^{-1}$ as a function of the concentrations of thiram in ethanol.

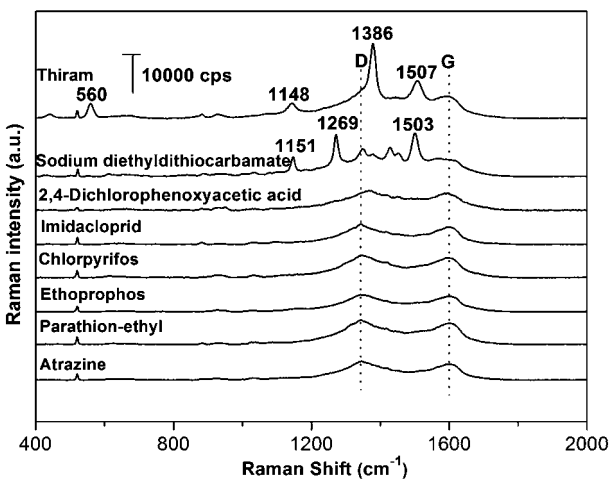


**Fig. 5** SERS spectra of various agricultural chemicals ($1 \times 10^{-5}$ M) applied on the Au@Ag NPs/GO/Au@Ag NPs sandwich structure, showing the highly selective Raman scattering enhancement for dithiocarbamates over other types of agricultural chemical.

to disperse the sample solution homogeneously on the sandwich substrate, 100 μL of the spiked sample solution was diluted in ethanol to 1 mL, and then 10 μL of the diluted solution was dropped onto the substrate. Fig. 6a is the Raman spectra of thiram in grape juice at different spiked concentrations increasing from $1.0 \times 10^{-7}$ to $1.0 \times 10^{-5}$ M on the sandwich structure, and the Raman intensity of thiram molecules at 560 $cm^{-1}$ increases with the thiram residue amount in the juice. Significantly, the detection limit of thiram in the grape juice is $1.0 \times 10^{-7}$ M, which is the same as the detection limit in ethanol. Similar results were obtained by a systematic study on the Raman response to thiram in ultrapure water and real lake water in the same conditions (Fig. S9, ESI†). Fig. 6b reflects the relationship between SERS intensity at 560 $cm^{-1}$ and the concentrations of the thiram in grape juice, ultrapure water and real lake water. All the fingerprint SERS signals of thiram could be observed clearly from the three samples. The results imply that the as-fabricated GO embedded sandwich structure can be used to detect thiram in all of the different matrices tested with high sensitivity and good reproducibility.

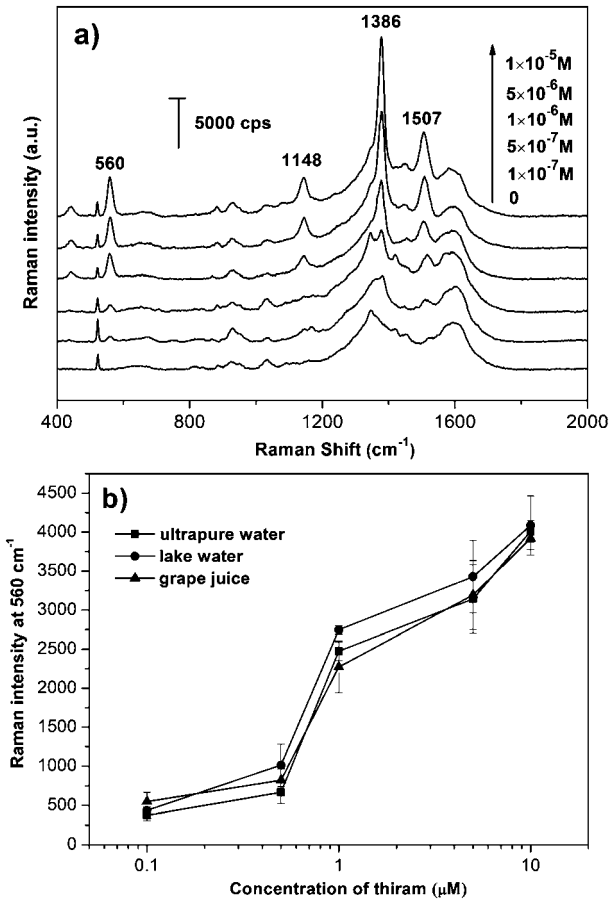


**Fig. 6** (a) SERS spectra of thiram in grape juice at different spiked concentrations on the Au@Ag NPs/GO/Au@Ag NPs sandwich structure. (b) The intensities of the SERS signals at 560 $cm^{-1}$ as a function of the concentrations of thiram spiked in different matrices of natural lake water, grape juice and ultrapure water.

## 4 Conclusion

In summary, we have developed a graphene oxide embedded sandwich structure through a simple self-assembly process as an effective SERS substrate. Significantly, the sandwich structure SERS substrate could produce highly enhanced Raman signals (EF $\sim 7.0 \times 10^7$) with good uniformity and reproducibility due to having plenty of hot spots on its surface and the unique structure of the graphene oxide sheets. The graphene oxide embedded sandwich nanostructure film can be applied to detect the pesticide thiram in commercial grape juice with a detection limit as low as 0.1 μM (0.03 ppm), which is about 2 orders of magnitude lower than the maximal residue limit (MRL) of 7 ppm in fruit prescribed by U.S. Environmental Protection Agency (EPA). The simple, rapid, and ultrasensitive Raman detection strategy using the graphene oxide embedded sandwich structure as a Raman amplifier exhibits great practical potential for the on-site monitoring of food/environmental safety and the spectroscopic identification of trace pesticides in agricultural products.

## Acknowledgements

This work was supported by the Natural Science Foundation of China (nos 61071055, 21077108, 21275145, 21277145) and the National Science & Technology Pillar Program (Grant 2012BAJ24B02).

## Notes and references

1 M. Fleischmann, P. J. Hendra and A. J. Mcquillan, *Chem. Phys. Lett.*, 1974, **26**, 163.

2 (*a*) L. Guerrini, J. V. Garcia-Ramos, C. Domingo and S. Sanchez-Cortes, *Anal. Chem.*, 2009, **81**, 1418; (*b*) J. P. Camden, J. A. Dieringer, Y. M. Wang, D. J. Masiello, L. D. Marks, G. C. Schatz and R. P. Van Duyne, *J. Am. Chem. Soc.*, 2008, **130**, 12616; (*c*) J. Jiang, K. Bosnick, M. Maillard and L. Brus, *J. Phys. Chem. B*, 2003, **107**, 9964.

3 (*a*) R. Y. Liu, B. H. Liu, G. J. Guan, C. L. Jiang and Z. P. Zhang, *Chem. Commun.*, 2012, **48**, 9421; (*b*) S. Abalde-Cela, S. Ho, B. Rodríguez-González, M. A. Correa-Duarte, R. A. Álvarez-Puebla, L. M. Liz-Marzán and N. A. Kotov, *Angew. Chem., Int. Ed.*, 2009, **48**, 5326; (*c*) L. F. He, J. N. Huang, T. T. Xu, L. M. Chen, K. Zhang, S. T. Han, Y. He and S. T. Lee, *J. Mater. Chem.*, 2012, **22**, 1370; (*d*) H. B. Zhou, Z. P. Zhang, C. L. Jiang, G. J. Guan, K. Zhang, Q. S. Mei, R. Y. Liu and S. H. Wang, *Anal. Chem.*, 2011, **83**, 6913; (*e*) Z. L. Huang, G. W. Meng, Q. Huang, Y. J. Yang, C. H. Zhu and C. L. Tang, *Adv. Mater.*, 2010, **22**, 4136; (*f*) H. K. Park, J. K. Yoon and K. Kim, *Langmuir*, 2006, **22**, 1626; (*g*) V. Liberman, C. Yilmaz, T. M. Bloomstein, S. Somu, Y. Echegoyen, A. Busnaina, S. G. Cann, K. E. Krohn, M. F. Marchant and M. Rothschild, *Adv. Mater.*, 2010, **22**, 4298.

4 (*a*) N. Jung, A. C. Crowther, N. Kim, P. Kim and L. Brus, *ACS Nano*, 2010, **4**, 7005; (*b*) X. Ling, L. M. Xie, Y. Fang, H. Xu,

 

H. L. Zhang, J. Kong, M. S. Dresselhaus, J. Zhang and Z. F. Liu, *Nano Lett.*, 2010, **10**, 553.

5 (*a*) X. Q. Fu, F. L. Bei, X. Wang, X. J. Yang and L. D. Lu, *J. Raman Spectrosc.*, 2010, **41**, 370; (*b*) W. Ren, Y. X. Fang and E. K. Wang, *ACS Nano*, 2011, **5**, 6425.

6 X. Ling, J. X. Wu, W. G. Xu and J. Zhang, *Small*, 2012, **8**, 1365.

7 (*a*) X. J. Liu, L. Y. Cao, W. Song, K. L. Ai and L. H. Lu, *ACS Appl. Mater. Interfaces*, 2011, **3**, 2944; (*b*) S. M. Maliyekkal, T. S. Sreeprasad, D. Krishnan, S. Kouser, A. K. Mishra, U. V. Waghmare and T. Pradeep, *Small*, 2013, **9**, 273.

8 (*a*) S. J. He, K. K. Liu, S. Su, J. Yan, X. H. Mao, D. F. Wang, Y. He, L. J. Li, S. P. Song and C. H. Fan, *Anal. Chem.*, 2012, **84**, 4622; (*b*) Y. Hu, L. H. Lu, J. H. Liu and W. Chen, *J. Mater. Chem.*, 2012, **22**, 11994; (*c*) C. Y. Liu, K. C. Liang, W. Chen, C. H. Tu, C. P. Liu and Y. Tzeng, *Opt. Express*, 2011, **19**, 17092; (*d*) G. Lu, H. Li, C. Liusman, Z. Y. Yin, S. X. Wu and H. Zhang, *Chem. Sci.*, 2011, **2**, 1817.

9 B. H. Liu, G. M. Han, Z. P. Zhang, R. Y. Liu, C. L. Jiang, S. H. Wang and M. Y. Han, *Anal. Chem.*, 2012, **84**, 255.

10 (*a*) V. K. Sharma, J. S. Aulakh and A. K. Malik, *J. Environ. Monit.*, 2003, **5**, 717; (*b*) A. K. Malik and W. Faubel, *Pestic. Sci.*, 1999, **55**, 965.

11 R. Krieger, A toxicological assessment of sulfur as a pesticide, in *Hayes' Handbook of Pesticide Toxicology*, ed. D. K. Gammon, T. B. Moore and M. A. O'Malley, Academic Press, New York, 2010, vol. 1, p. 1889.

12 (*a*) A. K. Malik and A. L. J. Rao, *Talanta*, 1990, **37**, 1205; (*b*) J. S. Aulakh, A. K. Malik and R. K. Mahajan, *Talanta*, 2005, **66**, 266; (*c*) C. Fernández, A. J. Reviejo, L. M. Polo and J. M. Pingarrón, *Talanta*, 1996, **43**, 1341; (*d*) V. K. Sharma, J. S. Aulakh and A. K. Malik, *Talanta*, 2005, **65**, 375; (*e*) O. M. S. Filipe, M. M. Vidal, A. C. Duarte and E. B. H. Santos, *Talanta*, 2007, **72**, 1235; (*f*) E. B. Rupp, P. Zuman, I. Šestáková and V. Horák, *J. Agric. Food Chem.*, 1992, **40**, 2016; (*g*) Y. G. Zhao, X. W. Zheng, Z. Y. Huang and M. M. Yang, *Anal. Chim. Acta*, 2003, **482**, 29.

13 P. C. Lee and D. Meisel, *J. Phys. Chem.*, 1982, **86**, 3391.

14 V. C. Tung, M. J. Allen, Y. Yang and R. B. Kaner, *Nat. Nanotechnol.*, 2009, **4**, 25.

15 (*a*) F. Schedin, E. Lidorikis, A. Lombardo, V. G. Kravets, A. K. Geim, A. N. Grigorenko, K. S. Novoselov and A. C. Ferrari, *ACS Nano*, 2010, **4**, 5617; (*b*) H. Q. Zhou, C. Y. Qiu, F. Yu, H. C. Yang, M. J. Chen, L. J. Hu and L. F. Sun, *J. Phys. Chem. C*, 2011, **115**, 11348; (*c*) J. Lee, S. Shim, B. Kim and H. S. Shin, *Chem.–Eur. J.*, 2011, **17**, 2381.

16 R. Mészáros, L. Thompson, M. Bos and P. de Groot, *Langmuir*, 2002, **18**, 6164.

17 C. Yuan, R. Y. Liu, S. H. Wang, G. M. Han, M. Y. Han, C. L. Jiang and Z. P. Zhang, *J. Mater. Chem.*, 2011, **21**, 16264.

18 J. S. Kang, S. Y. Hwang, C. J. Lee and M. S. Lee, *Bull. Korean Chem. Soc.*, 2002, **23**, 1604.